Applied Energy 329 (2023) 120201

Contents lists available at ScienceDirect

Applied Energy

journal homepage: www.elsevier.com/locate/apenergy

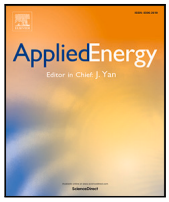

Data-driven scheme for optimal day-ahead operation of a wind/hydrogen system under multiple uncertainties☆

Yi Zheng [a], Jiawei Wang [a,*], Shi You [a], Ximei Li [a,c], Henrik W. Bindner [a], Marie Münster [b]

[a] Department of Wind and Energy Systems, Technical University of Denmark, 2800 Kgs. Lyngby, Denmark
[b] Department of Technology, Management and Economics, Technical University of Denmark, 2800 Kgs. Lyngby, Denmark
[c] School of Energy Science and Engineering, Harbin Institute of Technology, No. 92, West Dazhi Street, Harbin 150001, China

ARTICLE INFO

Keywords:
Data-driven
Robust optimization
Day-ahead operation
Wind/hydrogen system
DRCCP

ABSTRACT

Hydrogen is believed as a promising energy carrier that contributes to deep decarbonization, especially for the sectors hard to be directly electrified. A grid-connected wind/hydrogen system is a typical configuration for hydrogen production. For such a system, a critical barrier lies in the poor cost-competitiveness of the produced hydrogen. Researchers have found that flexible operation of a wind/hydrogen system is possible thanks to the excellent dynamic properties of electrolysis. This finding implies the system owner can strategically participate in day-ahead power markets to reduce the hydrogen production cost. However, the uncertainties from imperfect prediction of the fluctuating market price and wind power reduce the effectiveness of the offering strategy in the market. In this paper, we proposed a decision-making framework, which is based on data-driven robust chance constrained programming (DRCCP). This framework also includes multi-layer perception neural network (MLPNN) for wind power and spot electricity price prediction. Such a DRCCP-based decision framework (DDF) is then applied to make the day-ahead decision for a wind/hydrogen system. It can effectively handle the uncertainties, manage the risks and reduce the operation cost. The results show that, for the daily operation in the selected 30 days, offering strategy based on the framework reduces the overall operation cost by 24.36%, compared to the strategy based on imperfect prediction. Besides, we elaborate the parameter selections of the DRCCP to reveal the best parameter combination to obtain better optimization performance. The efficacy of the DRCCP method is also highlighted by the comparison with the chance-constrained programming method.

1. Introduction

Renewable hydrogen is regarded as a promising energy carrier for the sustainable energy transition. It can be produced by water splitting using electricity from various renewable energy resources. In this paper, we mainly discuss wind energy. Such a production pathway makes renewable hydrogen a womb-to-tomb green energy carrier. As a carbon-free fuel, it contributes to the deep decarbonization of a range of sectors, especially hard-to-abate ones (iron, steel, intensive transport) [1]. Converting renewable energy into hydrogen can also serve as a way for energy storage, enabling a high renewable energy penetration and offering flexibility to power systems [2].

Using renewable power can ensure the produced hydrogen is green, but the intermittence and fluctuation of renewable power result in low working hours of electrolysis [1,3]. A grid-connected wind/hydrogen system is another typical configuration to produce hydrogen. With this configuration, hydrogen is produced chiefly from wind power. At the same time, electricity from utility grids serves as an alternative in the case of insufficient wind power generation, which significantly raises the capacity factor of electrolysis [4]. Wind power can also be traded in electricity markets, bringing extra revenues. However, as investigated in [5], the cost of such hydrogen production is still much higher than the conventional fuel-based hydrogen (one from steam methane reforming). Researchers also find that the electricity cost plays an essential role in the production cost of the hydrogen [6,7]. Reducing electricity cost becomes an effective way to raise the cost competitiveness of the produced hydrogen.

The wind/hydrogen system owner can trade electricity by participating in day-ahead electricity markets (DAMs). As electrolysis capacity

☆ The short version of the paper was presented at ICAE2021, Nov. 29–Dec. 5, 2021. This paper is a substantial extension of the short version of the conference paper.

* Corresponding author.
E-mail addresses: yiazh@dtu.dk (Y. Zheng), jiawang@dtu.dk (J. Wang).

https://doi.org/10.1016/j.apenergy.2022.120201
Received 29 June 2022; Received in revised form 9 September 2022; Accepted 17 October 2022
Available online 4 November 2022

Nomenclature

Parameters

$p_b^{\text{ele}}, I_b^{\text{ele}}$	Power and current of electrolyzer at breakpoint b (kW, A)
v, p_t^w	Wind speed (m/s), wind power (MW)
$\dot{m}_t^{\text{Load}}$	Hydrogen load (kg/h)
η_f, F	Faraday efficiency and Faraday constant
η_{con}	Converter efficiency
$\hat{\pi}_t^{\text{ele}}$	Predicted electricity price (€/MWh)
ρ, A	Air density (kg/m^3), wind turbine swept area (m^2)
MW_{H_2}	Molar weight of hydrogen (kg/mol)
$\tilde{\pi}_t^{\text{ele}}$	Electricity price prediction error (€/MWh)
$\underline{I}, \overline{I}$	Lower and upper bound of electrolyzer current (A)
$C^{\text{HS}}, C^{\text{CS}}$	Hot start cost and cold start cost (€)
C_p	Power coefficient of wind turbine
n_s	Number of electrolyzer stack
P_s	Power consumption at stand-by state (kW)
p_t^L	Electricity loads (MW)
SoC_0	Initial SoC of hydrogen tank
v_r, p_r	Rated speed (m/s) and rated power (MW)
$v_{\text{ci}}, v_{\text{co}}$	Cut-in and cut-out speed (m/s)

Variables

$\dot{m}_t^{\text{by}}$	Hydrogen through bypass (kg/h)
$\dot{m}_t^{\text{ele}}$	Hydrogen from electrolyzer (kg/h)
$\dot{m}_t^{\text{ti}}, \dot{m}_t^{\text{to}}$	Inlet and outlet hydrogen of tank (kg/h)
p_t^b, s_t^b, i_t^b	Binary for production, standby and off states
p_t^u	Power purchased from utility grid (MW)
p_t^{comp}	Compressor power (MW)
p_t^{con}	Converter power (MW)
$p_t^{\text{ele}}, I_t^{\text{ele}}$	Electrolyzer power and current (kW, A)
p_t^{imb}	Real time imbalance (MW)
$s_t^{p,\text{ele}}, s_t^{I,\text{ele}}$	Slack variables
SoC_t	State of charge of hydrogen tank
$w_{b,t}$	Weight of breakpoint b
Y_t^b, Z_t^b	Binaries for hot start and cold start

is generally not large enough to influence market clearing, we assume that a wind/hydrogen system is a price-taker. One way to reduce the operation cost is to produce more hydrogen when the spot price is low and vice versa. Thanks to the high flexibility of electrolysis, this is possible because electrolysis power consumption can be quickly changed. In most DAMs, the offering curves of a wind/hydrogen system are submitted before the gate-closure on the previous day, e.g., noon in Nordpool [8]. Since the spot price has not been revealed when making decisions, the owner first needs to predict the spot price and then strategically submits the offers in DAMs. In this context, the owner faces imperfect prediction and uncertain prediction errors of the spot price. Another risk stems from the uncertain wind power prediction. As wind turbines are considered to be owned by the same owner, the wind power output should also be predicted before deciding the day-ahead (DA) offering strategy. A poor wind power prediction would lead to a significant imbalance in real-time operation, which will be penalized. For example, if the real-time delivered power is less than the contracted power in DAM, the system owner must pay for the deviation. To determine the penalty, different regulations of real-time market are adopted around the world [9]. This penalty should also be considered as an operation cost of a wind/hydrogen system.

Researchers have widely used stochastic and robust optimization (SO and RO) to cope with the uncertainties. The SO typically builds on scenarios. It seeks the decision variables that optimize the expected value of the objective function over a series of scenarios. In general, it assumes a probability distribution of the uncertain parameters and then generates scenarios of uncertainties following the distribution. Ref. [10] proposed a multi-stage SO for the design of a hydrogen supply chain network under uncertain demand. Jie Mei et al. studied a multi-energy system operation using SO to handle the uncertainties from solar power, and demand [11]. Conditional value at risk (CVaR) is frequently used along with SO to improve the robustness. The CVaR-based SO highlights the worse scenarios that result in high operation cost and gives more weight to the terms in the objective function related to these scenarios. In [12], the authors used CVaR to cope with the financial risks of grid-connected PV/hydrogen systems. The RO, on the other hand, is focused on the performance of the decisions in the worst-case scenario. This is achieved by introducing an uncertainty set that limits the range of uncertain parameters. B. Li et al. studied the optimal component sizing of an isolated microgrid considering uncertainties from loads and power outputs [13]. A polyhedron uncertainty set was used to represent the uncertainties. Diederik et al. investigated a renewable-powered hydrogen refueling station under techno-economic uncertainty using RO [14].

However, there are some disadvantages of SO and RO when addressing the uncertainties. It is believed that SO is biased towards the assumed distribution of the uncertainties, because the true distribution of uncertainties is unknown [15]. In addition, the SO becomes computationally burdensome as the number of scenarios grows [16]. In parallel, RO is too conservative against uncertainties due to the risk aversion [17]. In this context, data-driven robust optimization (DDRO) emerges as a way to bridge the gap between SO and RO. The DDRO builds on the concept of ambiguity set, a set that involves possible probability distribution of uncertain parameters [18]. In this paper, we focus on data-driven robust chance constrained programming (DRCCP), a type of DDRO. The DRCCP translates the constraints involving uncertainties into chance constrained form and seeks the decision variables to satisfy the chance constraints with a certain probability. Compared to SO, the DRCCP does not rely on pre-specified probability distribution and is more computationally tractable. Furthermore, compared to RO, the DRCCP extracts more information from historical data and gives a less conservative decision. It is one of the most suitable modeling paradigms to account for uncertainties in decision making [19].

Based on DRCCP, in this paper, we propose a framework for the optimal day-ahead operation of a wind/hydrogen system. The DRCCP-based decision framework (DDF) can tackle uncertainties from both wind power prediction and price prediction. The decisions from DDF can minimize the operation cost in the presence of risks. This work contributes to the state-of-the-art studies as follows: 1. We proposed a universal DDF for a wind/hydrogen system considering multiple uncertainties of wind power production and electricity prices. 2. The proposed framework is embedded with the function of short-term forecast, data collection and data pretreatment of uncertainties. Furthermore, the parameter selection of the proposed framework, DDF, is discussed in detail, which provides user-friendly instructions on the usage of such a framework. Besides, the framework is extendable, providing a good prototype to handle more uncertain parameters without too much modification. 3. The proposed framework is validated based on real-world system parameters and market data.

The remaining paper is organized as follows: Section 2 introduces the DDF, followed by the modeling of key components in Section 3. Section 4 expresses the day-ahead operation as an optimization problem. Section 5 further establishes the DRCCP form of the optimization and reformulates DRCCP as a tractable MILP problem. The simulation results are described and discussed in Section 6, and Section 7 concludes this work.

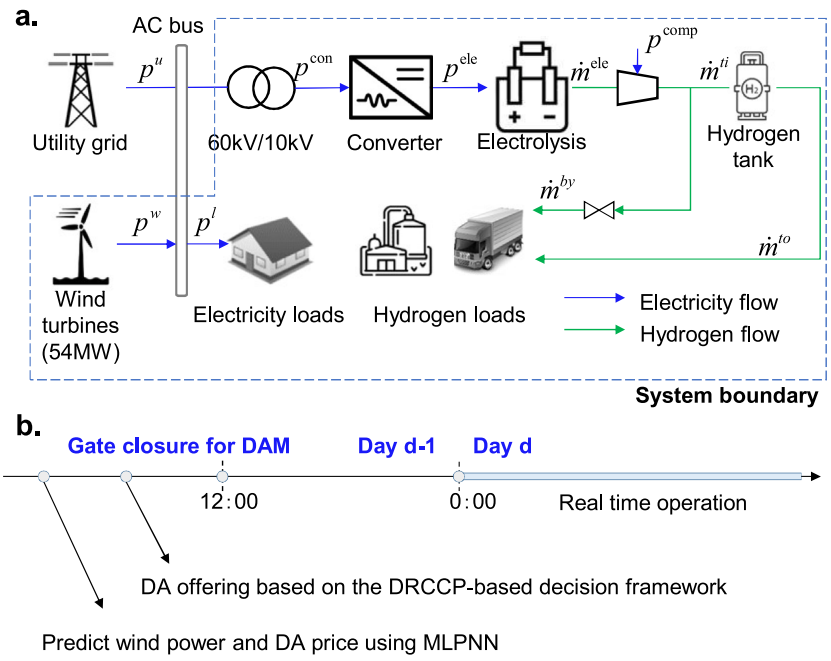

Fig. 1. (a) The schematics of the studied system. (b) Timeline of the system owner's participation in the electricity market.

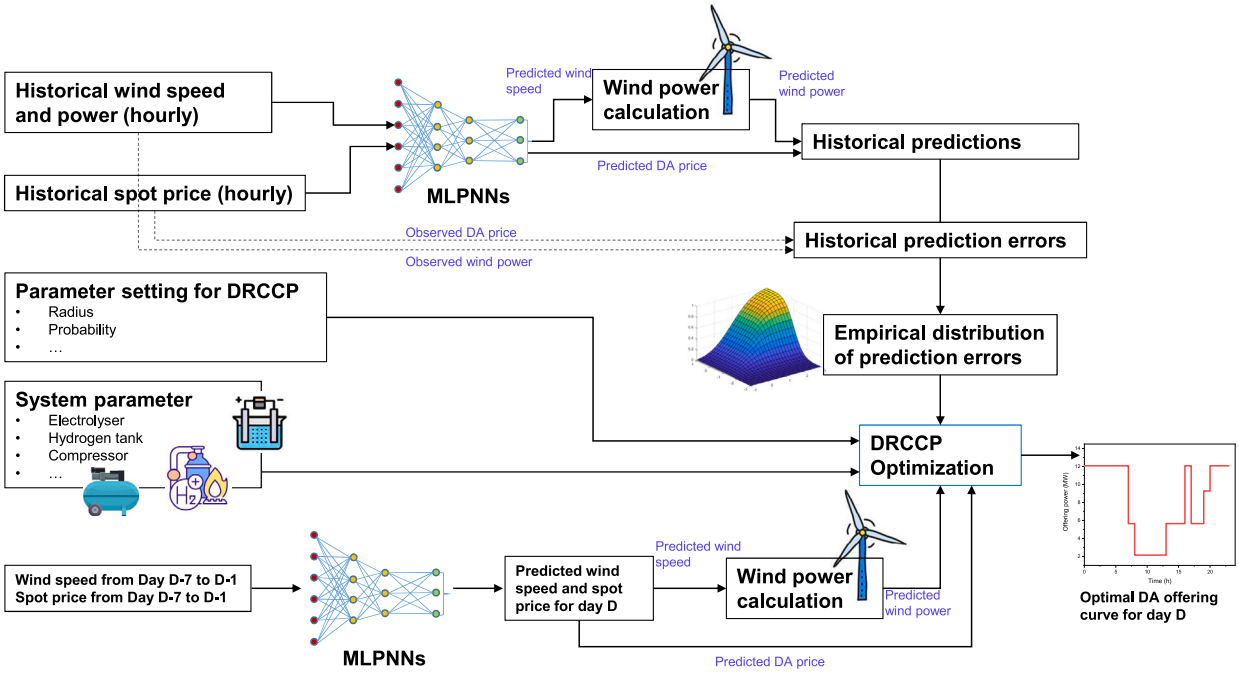

Fig. 2. The structure and data flow of the proposed DRCCP-based decision framework.

2. DRCCP-based decision framework

This section introduces the typical wind/hydrogen systems and then describes the proposed DDF. Fig. 1(a) delineates the configuration of the studied wind/hydrogen system, where the dashed line indicates the system boundary. Components within the boundary are considered to be owned by the same owner. The key component is the electrolyzer that converts DC power into hydrogen. The produced hydrogen is then compressed and delivered to the end-users. The hydrogen tank is used to decouple the production and loads, therefore enables flexible hydrogen production. The power required by the electrolysis is provided by the utility grid and wind farm. The wind power can also be traded in the electricity spot market. Fig. 1(b) describes the market behavior of the system owner. Before the gate closure of the DAM, the system owner needs to submit final offers to market operators, i.e. the energy that the owner will buy or sell for the next 24 h. To decide an optimal offering strategy, the system owner needs to predict the wind power and DA price for the next 24 h, and consider the uncertainties related to the predictions.

The DDF is proposed to assist the decision-making, and it primarily builds on a multi-layer perception neural network (MLPNN) prediction and DRCCP optimization. The structure and data flow of the DDF is presented in Fig. 2. The MLPNN is a complex network system formed by the extensive interconnection of many simple processing units (called

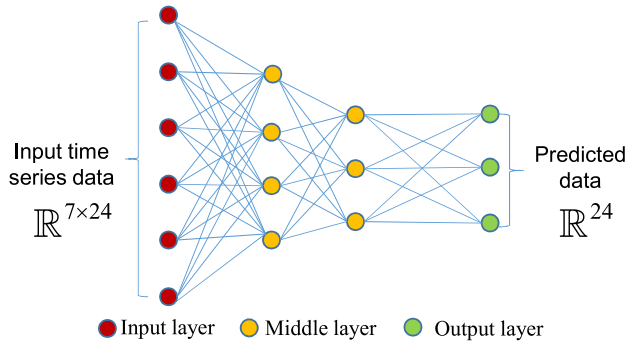

Fig. 3. Diagram of the utilized multi-layer perception neural network.

neurons). It is composed of an input layer, multiple middle layers, and an output layer. It is a flexible and powerful nonlinear model, as it can approximate virtually any function to any desired accuracy if given enough hidden neurons and enough data [20]. This paper uses the MLPNN model to predict the hourly electricity price and wind power. The previous seven-day time series data are used as the input, and the data for the next 24 h are predicted. The MLPNN is firstly trained over a training data set. The model weights are updated to create a good mapping of inputs and outputs in this process. The trained model with fitted parameters is then used for prediction. Fig. 3 demonstrates the structure of the MLPNN. Since the prediction method is not the focus of this paper, the details of the training process are not provided here. A detailed review on the topic can be found in [21].

On the other hand, the DRCCP optimization plays a critical role in this framework. The input of the DRCCP includes the wind/hydrogen system parameters, the DRCCP optimization parameters, the empirical distribution of prediction errors, and the predicted wind power and DA price. Among these inputs, it is important to highlight the formation of the empirical distribution. The wind power prediction error for a day is a vector in $\mathbb{R}^{24}$, with each element an hourly error. Hundreds of such vectors can be obtained from historical data, and these vectors form a sample set of daily wind power prediction error. Assuming the error, the 24-dimensional random vector, has a uniform distribution over the sample set, we then obtain an empirical discrete distribution of the prediction error. Besides, we need to set the key parameters (radius of Wasserstein ball and probability related to chance constraints) for the DRCCP to obtain better optimization performance. These parameters will be further discussed in the next sections. The DRCCP optimization finally gives the optimal offering curve for the next 24 h, as the output of the DDF.

3. System modeling

3.1. Wind turbines

A wind turbine converts kinetic energy into electric energy. It works in a limited wind speed range between the cut-in speed v_{ci} and the cut-out speed v_{co}. The power production of a wind turbine, denoted as $p^w(t)$, can be expressed by:

$$p^w(t)=\begin{cases}0, v<v_{\text{ci}}\\ \frac{v^3-v_{\text{ci}}^3}{v_r^3-v_{\text{ci}}^3}p_r, v_{\text{ci}}\le v<v_r\\ p_r, v_r\le v<v_{\text{co}}\\ 0, v_{\text{co}}\le v\end{cases} \tag{1}$$

where p_r is the rated power, kW; v_r is the rated wind speed, m/s; v is the wind speed at the blades height of a wind turbine, m/s, it can be calculated from the ground wind speed v_g:

$$\frac{v}{v_g}=\left(\frac{h}{h_g}\right)^{\alpha_h} \tag{2}$$

where h_g is the near-ground height, m; h is the height of wind turbine blades, m. α_h is the Hellman coefficient, usually between 0.128 and 0.160 [22].

3.2. Electrolyzers

Electrolyzers are the core energy conversion modules of a wind/hydrogen system. There are three types of electrolyzers: the alkaline, the proton-exchange membrane, and the high-temperature. The alkaline electrolyzer presently dominates the market for its low cost and large-scale applications. The electrode reactions and overall reaction are as below:

$$\text{Anode}: \quad 4OH^- = 2H_2O + O_2 + 4e^- \tag{3}$$

$$\text{Cathode}: \quad 2H_2O + 4e^- = 2OH^- + H_2 \tag{4}$$

$$\text{Overall reaction}: \quad 2H_2O = O_2 + 2H_2 \tag{5}$$

For an electrolyzer model, the key is to reveal the relationship between input power and output hydrogen production rate. The simplest assumption is that electrolyzers have fixed efficiency and hydrogen conversion rate (for example, 20 kg/MWh). This assumption, however, is believed not realistic because a higher conversion rate is observed in the case of partial loading. Meanwhile, an electrolyzer generally has a limitation for its lowest working current due to different reasons, e.g. safety considerations. An alkaline electrolyzer can adjust its load in the range of 15% to 100%, which is another critical operation limit. Besides, an electrolyzer's operation has three operation states (production, standby and idle) and has different properties in these states, which should also be highlighted in its operation planning. In our previous work [23], we elaborate these properties and give detailed mathematical descriptions. We inherit our electrolyzer models and further consider efficiency variation (by piece-wise linearization), as well as state transitions in this work.

For the converter, compressor and hydrogen tank, we use simplified mathematical models, which can be found in the next section.

4. Problem formulation

The core of the proposed DDF is the DRCCP optimization. In this section, we firstly formulate the day-ahead operation problem into mixed-integer programming (MILP) involving uncertain parameters. Then in the next section, we further handle the uncertainties using the DRCCP scheme. The system owner of a wind/hydrogen system aims at minimizing the overall daily cost for producing a specific amount of hydrogen. The objective function is expressed as follows:

$$\begin{aligned}\min_{\mathbf{x}} \quad & \sum_{t=1}^{T}((\hat{\pi}_t^{\text{ele}}+\tilde{\pi}_t^{\text{ele}})p_t^u+\alpha p_t^{\text{imb}})\\ & +\sum_{t=1}^{T-1}(C^{\text{HS}}Y_t^b+C^{\text{CS}}Z_t^b)\end{aligned} \tag{6}$$

where the first summation includes the cost of trading electricity in the day-ahead market and the penalty resulted from real-time imbalance. $\hat{\pi}_t^{\text{ele}}$ represents the predicted DA price for hour t while $\tilde{\pi}_t^{\text{ele}}$ is the uncertain price prediction error. p_t^{imb} denotes the deviation between the contracted power in DA market and the delivered power in real-time operation, as defined in Eq. (7); α is the constant penalty factor. This work utilizes a penalty calculation similar to the settings in [9]. The second summation represents the startup cost of the electrolyzer for both hot and cold starts.

$$p_t^{\text{imb}}=|p_t^{\text{con}}+p_t^L+p_t^{\text{comp}}-p_t^u-\hat{p}_t^w-\tilde{p}_t^w| \tag{7}$$

The decision variables are integrated as a vector $\mathbf{x}$:

$$\mathbf{x} = [\mathbf{p}^u, \mathbf{p}^{\text{imb}}, \mathbf{p}^{\text{comp}}, \mathbf{p}^{\text{con}}, \mathbf{p}^{\text{ele}}, \mathbf{I}^{\text{ele}}, \mathbf{w}_b, \mathbf{s}^{p,\text{ele}}, \mathbf{s}^{I,\text{ele}}, \mathbf{s}^b, \mathbf{i}^b, \mathbf{p}^b, \mathbf{Y}^b, \mathbf{Z}^b, \dot{\mathbf{m}}^{\text{by}}, \dot{\mathbf{m}}^{\text{ti}}, \dot{\mathbf{m}}^{\text{to}}, \dot{\mathbf{m}}^{\text{ele}}] \tag{8}$$

Unlike the two-stage optimization scheme (taking into account of both day-ahead and real-time market), all the variables above are "here and now", i.e., no "wait and see" variables. The data-driven method could also be used for a two-stage scheme, while to keep the problem simple and remain the key features of the data-driven method, we only focus on the day-ahead decision-making.

Electrolyzers bear several important operational characteristics that have to be considered in the short-term operation. The key challenges for modeling electrolyzers are the non-linear relationship between hydrogen production and power input, as well as the state transition properties of electrolyzers' operation. Constraints (9) to (17) express the relationship between the current load and power input:

$$p_t^{\text{ele}} = \sum_{b=1}^{N_b} w_{b,t} p_b^{\text{ele}} + s_t^{p,\text{ele}} \tag{9}$$

$$I_t^{\text{ele}} = \sum_{b=1}^{N_b} w_{b,t} I_b^{\text{ele}} + s_t^{I,\text{ele}} \tag{10}$$

$$-M(s_t^b + i_t^b) \le s_t^{p,\text{ele}} \le M(s_t^b + i_t^b) \tag{11}$$

$$-M(s_t^b + i_t^b) \le s_t^{I,\text{ele}} \le M(s_t^b + i_t^b) \tag{12}$$

$$\sum_{b=1}^{N_b} w_{b,t} = 1 \tag{13}$$

$$w_{1,t} \le z_{1,t} \tag{14}$$

$$w_{b,t} \le z_{b-1,t} + z_{b,t}, \quad \forall 2 \le b < N_b \tag{15}$$

$$w_{N_b,t} \le z_{N_b,t} \tag{16}$$

$$\sum_{b=1}^{N_b} z_{b,t} = 1 \tag{17}$$

Eqs. (9) and (10) are the piecewise representation of electrolyzer power consumption p_t^{ele} and current I_t^{ele}, where the slack variables $s_t^{p,\text{ele}}$ and $s_t^{I,\text{ele}}$ are adopted to decouple their relation if the electrolyzer works in the standby and off states. These slack variables $s_t^{p,\text{ele}}, s_t^{I,\text{ele}}$ are almost unbounded if either the standby or off state indicator is one, as presented in inequalities (11) and (12), where M is a sufficiently large constant. The $w_{b,t}$ in Eqs. (9) and (10) belongs to a special ordered set of type two, in which at most two adjacent components are positive. This special set can be established by constraints (13) to (17) through introducing the ancillary continuous and binary variables. The detailed formulation of the piecewise linear methods refers to [24]. The following constraints define the three states (production, standby and idle states, p_t^b, s_t^b and i_t^b) and hot/cold starts Y_t^b, Z_t^b:

$$p_t^b + s_t^b + i_t^b = 1 \tag{18}$$

$$p_t^b \underline{\mathbf{I}} \le I_t^{\text{ele}} \le p_t^b \overline{\mathbf{I}} \tag{19}$$

$$s_t^b \mathrm{P}_s \le p_t^{\text{ele}} \le p_t^b \mathrm{M}_1 + s_t^b \mathrm{P}_s \tag{20}$$

$$s_t^b + i_{t-1}^b \le 1, \quad \forall t \ge 2 \tag{21}$$

$$Y_{t-1}^b = s_{t-1}^b p_t^b, \quad \forall t \ge 2 \tag{22}$$

$$Z_{t-1}^b = i_{t-1}^b p_t^b, \quad \forall t \ge 2 \tag{23}$$

Eq. (18) enforces that the three states are incompatible. Inequality (19) defines the current range for the electrolyzer. Constraint (20) argues that the electrolyzer's power is P_s in the standby state, and is zero in the off state. Constraint (21) prevents the transition from the standby state to the off state, which is nonprofitable [25]. The next two equations are the definitions of the hot and cold start. Although both equations are non-linear, they could be easily linearized without adding extra binary variables, as shown in the following expressions:

$$0 \le Y_{t-1}^b \le p_t^b \tag{24}$$

$$0 \le s_{t-1}^b - Y_{t-1}^b \le 1 - p_t^b \tag{25}$$

$$0 \le Z_{t-1}^b \le p_t^b \tag{26}$$

$$0 \le i_{t-1}^b - Z_{t-1}^b \le 1 - p_t^b \tag{27}$$

It should be highlighted that Eqs. (22) and (23) are applicable only when the hot/cold start processes can complete within an hour. The hot start usually takes a few minutes [26]. The cold start, however, can take 20 min to several hours [27]. To simplify the constraints, we assume that the cold start time is less than one hour in this paper.

In the system level, the power imbalance p_t^{imb} and power consumption of the electrolyzer and the compressor are quantified as:

$$p_t^{\text{imb}} = max(p_t^{\text{con}} + p_t^L + p_t^{\text{comp}} - p_t^u - \hat{p}_t^w - \tilde{p}_t^w, 0) \tag{28}$$

$$\underline{p^u} \le p_t^u \le \overline{p}^u \tag{29}$$

$$p_t^{\text{con}} \eta_{\text{con}} = n_s p_t^{\text{ele}} \tag{30}$$

$$p_t^{\text{comp}} = \beta \dot{m}^{\text{ele}} \tag{31}$$

In this work, we assume that the wind curtailment is permitted, and its cost is ignored. Therefore, the real-time imbalance in (7) can be expressed by Eq. (28). p_t^{imb} is positive if the overall power consumption is greater than the power supply (from wind turbines $\hat{p}_t^w + \tilde{p}_t^w$ and utility grid p_t^u); zero if the supply is greater. Eq. (28), in essence, is again a piecewise linear function, which could be handled by introducing binary variables $z_{\text{lps},t}$. In this way, we are able to replace this constraint with inequalities (32) to (35). Constraint (29) represents the limited transmission line capacity. Constraint (30) links the converter power p_t^{con} with electrolyzer power p_t^{ele}, and Eq. (31) links the compressor power consumption p_t^{comp} with the hydrogen production rate $\dot{m}_t^{\text{ele}}$.

$$p_t^{\text{imb}} \ge p_t^{\text{con}} + p_t^L - p_t^u - \hat{p}_t^w - \tilde{p}_t^w \tag{32}$$

$$p_t^{\text{imb}} \ge 0 \tag{33}$$

$$p_t^{\text{imb}} \le z_{\text{lps},t} M_2 + p_t^{\text{con}} + p_t^L - p_t^u - \hat{p}_t^w - \tilde{p}_t^w \tag{34}$$

$$p_t^{\text{imb}} \le (1 - z_{\text{lps},t}) M_2 \tag{35}$$

Finally, we have the hydrogen demand balance presented in Eqs. (36) to (41). Eq. (36) gives the Faraday principle that links electrolyzer current I_t^{ele} with hydrogen production rate $\dot{m}_t^{\text{ele}}$. Constraints (37) and (38) are the mass balance of the hydrogen produced by electrolysis and hydrogen supplied to the loads, respectively. Eq. (39) describes the SoC changes in the hydrogen tank, followed by SoC's boundaries. The final equation states that the SoC level should remain the same at the start and end of the operation period.

$$\dot{m}_t^{\text{ele}} = 3600 \eta_f \mathrm{MW}_{\mathrm{H}_2} \frac{n_s I_t^{\text{ele}}}{2F} \tag{36}$$

$$\dot{m}_t^{\text{ele}} = \dot{m}_t^{\text{by}} + \dot{m}_t^{\text{ti}} \tag{37}$$

$$\dot{m}_t^{\text{by}} + \dot{m}_t^{\text{to}} = \dot{\mathrm{m}}_t^{\text{load}} \tag{38}$$

$$M^{\text{Ht}}(SoC_t - SoC_{t-1}) = \dot{m}_t^{\text{ti}} - \dot{m}_t^{\text{to}} \tag{39}$$

$$\underline{SoC} \le SoC_t \le \overline{SoC} \tag{40}$$

$$SoC_0 = SoC_T \tag{41}$$

For notational simplicity, we denote the uncertain parameters $\tilde{\boldsymbol{\pi}}^{\text{ele}}$ and $\tilde{\mathbf{p}}^w$ by $\boldsymbol{\xi}$ and $\boldsymbol{\zeta}$ respectively. The optimization problem could be

written in a compact way:

$$\begin{aligned} \min_{\mathbf{x}} \quad & \mathbf{c}^{\mathrm{T}}\mathbf{x} + \boldsymbol{\xi}^{\mathrm{T}}\mathbf{p}^{u} \\ s.t. \quad & \mathbf{x} \in \chi \\ & p_t^{\mathrm{imb}} \geq p_t^{\mathrm{con}} + p_t^{L} - p_t^{u} - \hat{p}_t^{w} - \zeta_t \\ & p_t^{\mathrm{imb}} \leq z_{\mathrm{lps},t} M_2 + p_t^{\mathrm{con}} + p_t^{L} - p_t^{u} - \hat{p}_t^{w} - \zeta_t \end{aligned} \tag{42}$$

where χ includes constraints (9) to (41) excluding inequalities (32) and (34) that contain uncertain parameters. All the constraints are linear and therefore the whole optimization problem is a MILP, which could be solved using mature algorithms and solvers. Remarkably, the optimal value of the problem (42) is not necessarily the true cost in real-time operation. In fact, the optimal solution of (42) gives a DA offering strategy. The actual operation cost should be calculated after the realization of uncertainties.

5. DRCCP reformulation

Uncertain parameters still exist in the problem (42), therefore in this section, we cope with the uncertainties using the DRCCP scheme. A new variable d is introduced so that all the uncertainties are included in the constraints, and the objective function is certain. This reformulation is widely used in robust optimization [28]. We lose nothing by doing this, and the new problem is equivalent to the problem (42), shown as follows:

$$\begin{aligned} \min_{\mathbf{x}\in\chi, d} \quad & \mathbf{c}^{\mathrm{T}}\mathbf{x} + d \\ s.t. \quad & \boldsymbol{\xi}^{\mathrm{T}}\mathbf{p}^{u} - d \leq 0 \\ & p_t^{\mathrm{imb}} \geq p_t^{\mathrm{con}} + p_t^{L} - p_t^{u} - \hat{p}_t^{w} - \zeta_t \\ & p_t^{\mathrm{imb}} \leq z_{\mathrm{lps},t} M_2 + p_t^{\mathrm{con}} + p_t^{L} - p_t^{u} - \hat{p}_t^{w} - \zeta_t \end{aligned} \tag{43}$$

It is noted that we have $1 + 2T$ constraints in this formulation. We then rewrite these constraints into chance constraints:

$$\mathbb{P}_1[\boldsymbol{\xi} \in S_1(\mathbf{x}, d)] \geq 1 - \epsilon_1, \quad \forall \mathbb{P}_1 \in \Gamma_{\hat{\mathbb{P}}_1}(\theta_1) \tag{44}$$

$$\mathbb{P}_2[\boldsymbol{\zeta} \in S_2(\mathbf{x}, d)] \geq 1 - \epsilon_2, \quad \forall \mathbb{P}_2 \in \Gamma_{\hat{\mathbb{P}}_2}(\theta_2) \tag{45}$$

For any selection of the decision variables $\mathbf{x}$ and d, $S_1(\mathbf{x}, d)$ is called the safety set of $\boldsymbol{\xi}$. If the realization of the uncertain parameter $\boldsymbol{\xi}$ falls within the safety set, $\mathbf{x}$ and d are feasible solutions. However, $\boldsymbol{\xi}$ is not always in S_1. Constraint (44) claims that $\boldsymbol{\xi}$ falls in S_1 with a probability larger than $1-\epsilon_1$ for any probability distribution $\mathbb{P}_1$ of $\boldsymbol{\xi}$ that is "close" to the empirical distribution $\hat{\mathbb{P}}_1$. The distance between two probability d_w is calculated based on Wasserstein metrics and $\Gamma_{\hat{\mathbb{P}}_1}(\theta_1)$ represents a Wasserstein ball centering on $\hat{\mathbb{P}}_1$ with radius of θ_1, which is defined as follows:

$$\Gamma_{\hat{\mathbb{P}}_1}(\theta_1) = \{\mathbb{P}_1 | d_w(\mathbb{P}_1, \hat{\mathbb{P}}_1) \leq \theta_1\} \tag{46}$$

Constraint (45) is formulated in a similar way, while it contains $2T$ individual constraints. Such constraint that involves multiple uncertain constraints is termed a joint chance constraint [29]. S_1 and S_2 can be expressed in compact forms as:

$$S_1(\mathbf{x}, d) = \{\boldsymbol{\xi} | \boldsymbol{\xi}^{\mathrm{T}}\mathbf{p}^{u} - d \leq 0\} \tag{47}$$

$$S_2(\mathbf{x}, d) = \{\mathbf{a}_m^T\mathbf{x} \leq \mathbf{b}_m^T\boldsymbol{\zeta} + b_m, \ \forall m \in \{1, 2, \ldots, 2T\}\} \tag{48}$$

We have the final DRCCP optimization as:

$$\begin{aligned} \min_{\mathbf{x}\in\chi, d} \quad & \mathbf{c}^{\mathrm{T}}\mathbf{x} + d \\ s.t. \quad & (44) \text{ and } (45) \end{aligned} \tag{49}$$

Zhi Chen et al. demonstrate that individual chance constraint, as well as a joint chance constraint with only right-hand uncertainty, are both mixed-integer representative [30]. The reformulation amounts to mixed-integer linear or conic programming. According to proposition 1 and 2 in Section 2.3 of [30], problem (49) is equivalent to the following optimization:

$$\begin{aligned} \min_{\substack{\mathbf{x}\in\chi, d, \mathbf{q}_1, \mathbf{s}_1, t_1 \\ \mathbf{p}_2, \mathbf{q}_2, \mathbf{s}_2, t_2}} \quad & \mathbf{c}^{\mathrm{T}}\mathbf{x} + d \\ s.t. \quad & \epsilon_1 N t_1 - \mathbf{e}^T\mathbf{s}_1 \geq \theta_1 N \|\mathbf{p}^u\|_* \\ & - \hat{\boldsymbol{\xi}}_i^T\mathbf{p}^u + d + M_3 q_{1,i} \geq t_1 - s_{1,i}, \ \ \forall i \in [N] \\ & M_3(1 - q_{1,i}) \geq t_1 - s_{1,i}, \ \ \forall i \in [N] \\ & \mathbf{q}_1 \in \{0,1\}^N, \mathbf{s}_1 \geq 0 \\ & \epsilon_2 N t_2 - \mathbf{e}^T\mathbf{s}_2 \geq \theta_2 N \\ & p_{2,i} + M_4 q_{2,i} \geq t_2 - s_{2,i} \ \ \forall i \in [N] \\ & M_4(1 - q_{2,i}) \geq t_2 - s_{2,i} \ \ \forall i \in [N] \\ & \mathbf{q}_2 \in \{0,1\}^N, \mathbf{s}_2 \geq 0 \\ & \frac{\hat{\zeta}_{i,t} + (-p_t^L + \hat{p}_t^w) - (-p_t^{\mathrm{lps}} + p_t^{\mathrm{con}} - p_t^u)}{\| -p_t^L + \hat{p}_t^w \|_*} \geq p_{2,i} \\ & \frac{-\hat{\zeta}_{i,t} + (p_t^L - \hat{p}_t^w) - (p_t^{\mathrm{lps}} - p_t^{\mathrm{con}} + p_t^u - M_2 z_{\mathrm{lps},t})}{\| p_t^L - \hat{p}_t^w \|_*} \geq p_{2,i} \end{aligned} \tag{50}$$

where N is the number of the samples, i.e., historical observation of uncertain parameters. $[N]$ represents a set $\{1, 2, \ldots, N\}$. $\mathbf{e}^T$ denotes the unit vector in $\mathbb{R}^N$. $\hat{\boldsymbol{\xi}}_i$ (in $\mathbb{R}^N$) and $\hat{\boldsymbol{\zeta}}_i$ (in $\mathbb{R}^N$) are the ith observation of price and wind power prediction errors, respectively. The number of samples of $\boldsymbol{\xi}$ and $\boldsymbol{\zeta}$ is not necessarily identical. Here, w.l.o.g we assume that the two sample sets share the same size. Each $M_{(.)}$ is a suitably large positive constant. While most of the constraints are linear and convex, the first inequality involving $\| p^u \|$ is non-linear and non-convex. Here, we refer $\| \cdot \|_*$ to $\| \cdot \|_1$ and the constraint could be expressed as:

$$\epsilon_1 N t_1 - \mathbf{e}^T\mathbf{s}_1 \geq \theta_1 N \sum_{t=1}^{T} |p_t^u| \tag{51}$$

This constraint could be linearized by letting $p_t^{u,a} := |p_t^u|$ and adding the following new constraints:

$$0 \leq p_t^{u,a} - p_t^u \leq 2M_5 u_t^b \tag{52}$$

$$M_5(1 - u_t^b) \geq p_t^u \tag{53}$$

$$0 \leq p_t^{u,a} + p_t^u \leq 2M_5(1 - u_t^b) \tag{54}$$

$$-M_5 u_t^b \leq p_t^u \tag{55}$$

$$-M_5 \leq p_t^u \leq M_5 \tag{56}$$

with u_t^b a binary variable and M_5 a large positive constant. The inequality constraint (51) is now replaced by constraints (52) to (56). Problem (50) only contains linear and convex constraints, which could be solved using MILP solvers. In this work, we solved this problem using Gurobi solver under the pyomo framework of Python. The problem scale is not large thanks to the advantage of the DRCCP. If the sample number is 100, for example, there are 1081 variables (416 binary variables and 665 continuous variables) and 6040 constraints and such a problem can be solved within 28.11s.

6. Results and discussion

6.1. System parameters

This paper builds a case study based on a real-life application, GreenLab Skive, an industrial park located in Denmark with several wind turbines, electrolyzers and chemical plants. The primary electricity and hydrogen consumption come from industrial plants, including a plastic pyrolysis plant, a methanol synthesis plant etc. Those demands

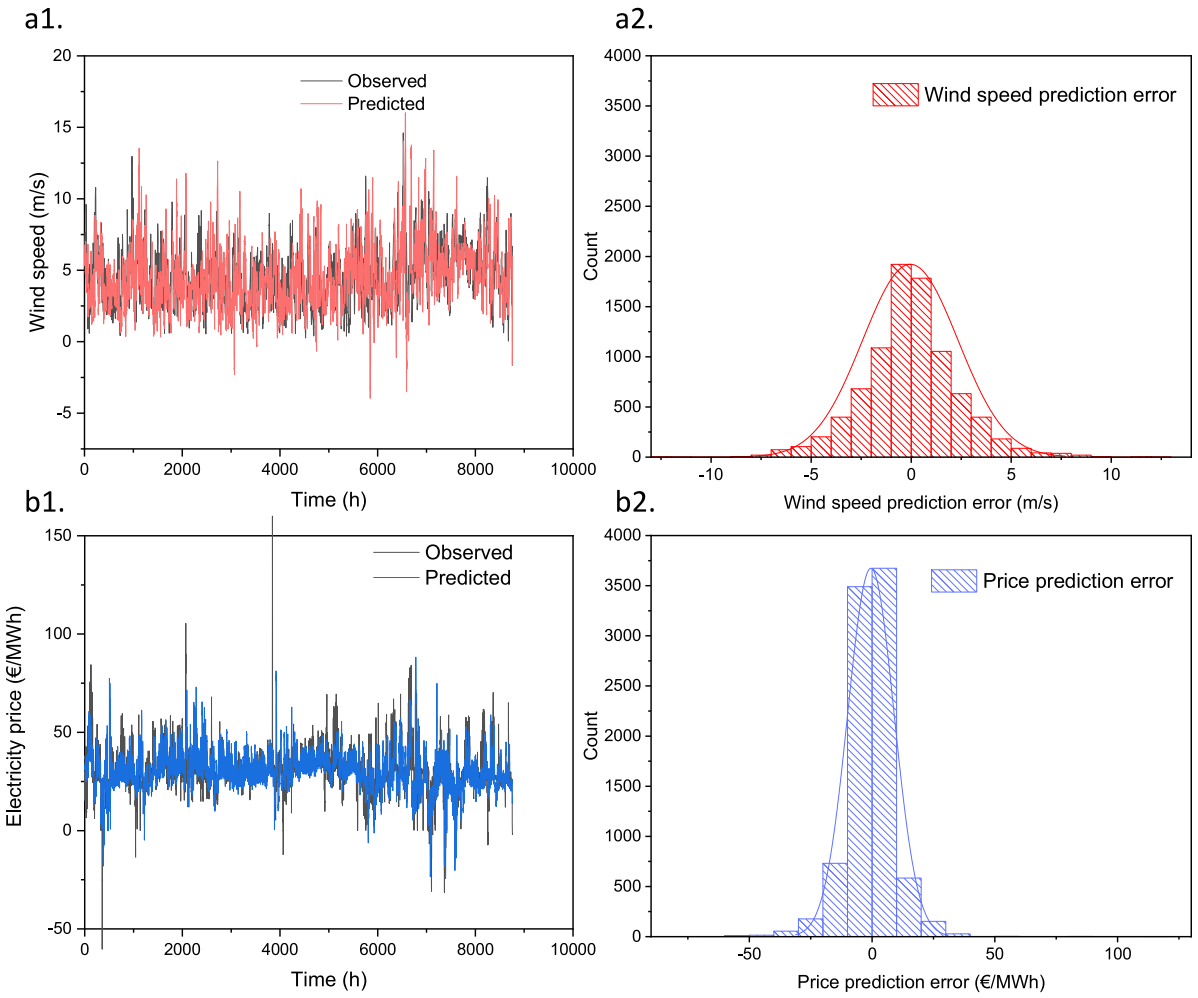

Fig. 4. (a1) wind speed prediction and observed wind speed over a year. (a2) the distribution of wind speed prediction errors. (b1) electricity price prediction and observed electricity price over a year. (b2) the distribution of electricity price prediction errors.

are pretty stable due to the fixed schedule of the production, and can be viewed as deterministic parameters in the optimization. The daily loads are presented in Appendix A. Thirteen wind turbines with a nominal capacity of 4.2 MW are installed, and 31 electrolyzers with the nominal production rate of 90 N m^3/h (i.e. 8.1 kg/h) are deployed. The total installed capacity of electrolyzers is around 12 MW. These capacities are pre-specified by the planner and are considered to be known in the analysis. No data for hydrogen storage is available. Here, we assume that hydrogen storage capacity is 6000 kg, nearly two days' consumption of the hydrogen in this park. For more technical details of the system, please refer to Appendix B.

The system owner needs to make decisions (offering strategy in the day-ahead market) based on the price and wind power prediction. Fig. 4 illustrates the prediction results over a whole year where the distribution of the prediction errors is also provided. One could see that the prediction is accurate for most days, while can also give a wrong "suggestion". The prediction errors approximately follow a normal distribution, and they can be substantial in some cases. Decisions on these poor predictions may result in penalty caused by a significant imbalance in real-time operation and the opportunity cost of energy arbitrage.

6.2. Deterministic optimization

To reveal how the uncertain prediction induces an extra cost, we first consider two deterministic scenarios. In the first scenario, we make the decisions based on the imperfect prediction and do not consider uncertainties. In the second scenario, the actual observed DA price and wind power are adopted, which results in a perfect solution as a good baseline for further comparison.

Fig. 5(a) illustrates the actual cost and the daily real-time energy imbalance during a seven-day simulation. Decisions made based on the imperfect predictions result in higher operation cost. For days 1, 3, 4, 5 and 6, the induced extra cost is not very large. This observation implies that the prediction is acceptable these days. However, for days 2 and 7, a sizeable real-time imbalance and high cost are observed. To further understand how this happens, Fig. 5(b) provides the price prediction for day seven. The observed prices, in general, is greater than the predicted ones, but the difference is within 5 €/MWh. Besides, the expected price trend is consistent with the observed one, therefore, it is unlikely that the price prediction error causes the high cost.

On the other hand, as shown in Fig. 5(c), the wind power prediction for this specific day is inaccurate. The predicted wind power trend is similar to the observed one, but the prediction is over-optimistic on wind power output. The operation strategy is made based on the expectation of high wind power output, but in reality, wind power is insufficient, leading to real-time imbalance. Further insights are provided in Fig. 5(d), the offering curve of this system. Compared to the case of perfect prediction, during hours 10 to 15, the offering curve based on imperfect prediction shows a lower demand. That is to say, the system owner expects little energy from the market in this period. However, wind power is not sufficient in real-time operation, implying that the actual energy demand is much higher than the contracted

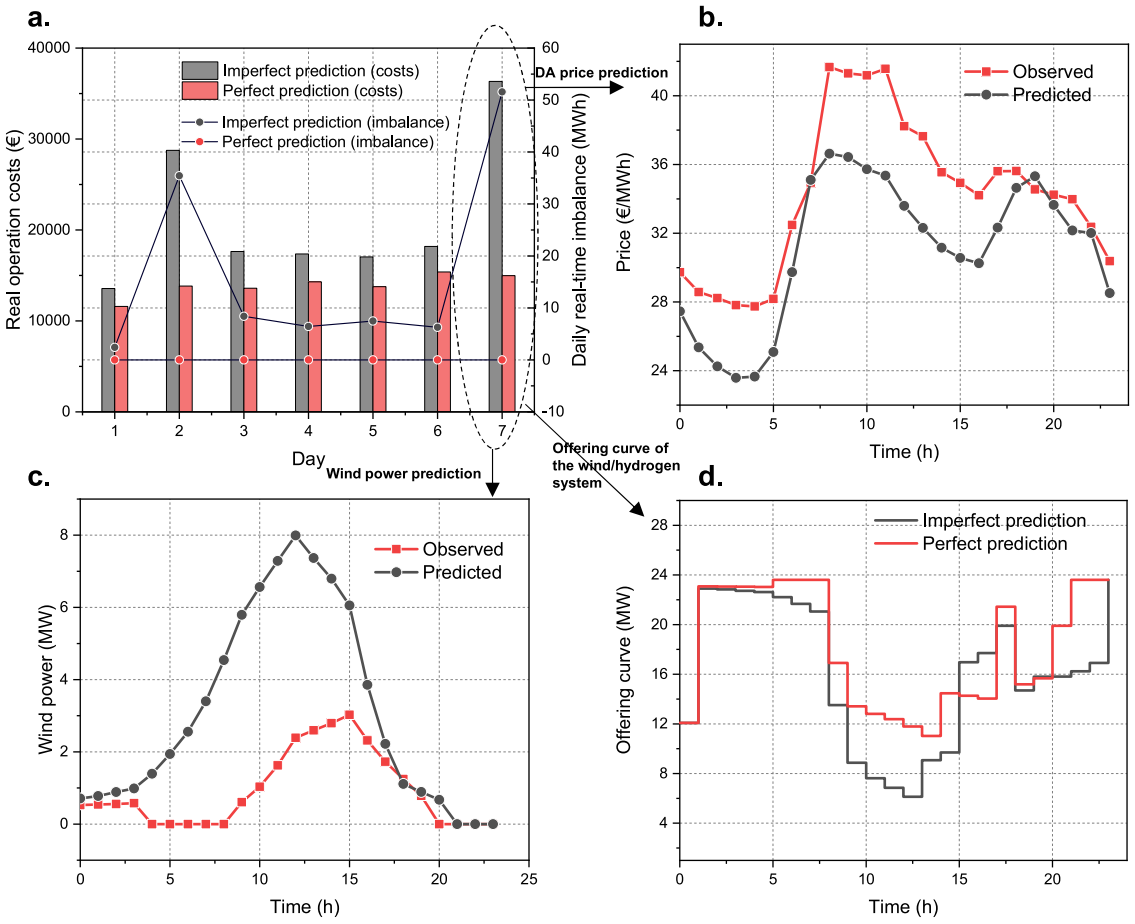

Fig. 5. (a) Real operation cost and real-time energy imbalance during the seven-day operation. Both the results based on imperfect and perfect prediction are given. (b) Predicted DA price vs observed DA price on day 7. (c) Predicted wind power vs observed wind power on day 7. (d) The offering curve of the wind/hydrogen system, i.e., the planned power exchange in DA market.

energy, leading to a significant imbalance in real-time operation and causing a penalty. The real-time imbalance for day seven is about 50 MWh. This analysis indicates that decisions based only on prediction may result in poor performance. It is vital to reduce the risks by considering extreme cases, i.e. significant prediction errors.

6.3. DRCCP optimization

To improve the performance of the decisions based on imperfect prediction, the data-driven method is utilized. By considering the historical observation of prediction errors, we obtain the new choices that depend not only on the day-ahead prediction but also on the available data of observed prediction errors. Both the price and wind power prediction uncertainties are handled. The values of the key parameters in constraints (44) and (45) are set as: $\theta_1 = 0.01$, $\theta_2 = 0.001$, $\epsilon_1 = 0.1$ and $\epsilon_2 = 0.05$. The selection of these values will be further discussed in the next section.

To verify the effectiveness of the proposed DRCCP optimization, we investigate the actual daily cost during the consecutive 30 days (including the seven days mentioned in Fig. 5) as well as the associated real-time imbalance. On the whole, it is found from Fig. 6 that the strategies based on the data-driven method reduce the actual cost significantly for most days. The cost reduction is considerable for days 2, 7, 13, 22 etc. when prediction is relatively poor. For example, on day 7, the actual cost for imperfect prediction is 36 330€, while the optimal cost is theoretically 14 979€. Because of the poor prediction, the operation strategy is far from optimum. Using the data-driven method considerably brings down the cost by 19 035€.

Further insights on how the data-driven method improves economics is provided in Fig. 7, where the real-time imbalance is presented. For day 7, the original imbalance reaches nearly 50 MWh and declines to 10 MWh given the robust decision. A significant imbalance and a hefty penalty are expected to be avoided. For most of the days, the real-time imbalance is almost zero.

On the other hand, the robust decision is ineffective for the days with good prediction, such as days 3, 4, 5, 6 etc. Unfortunately, we also observe that the robust decision could result in higher cost, e.g., on days 1, 8, 9 etc. The prediction is highly accurate on these specific days. However, we tend to be conservative and lose the opportunity of energy arbitrage.

Table 1 presents the total operation cost and real-time imbalance induced by different decision making framework. Overall, for the studied 30 days, the total operation cost is reduced by 24.36% using the data-driven method in comparison with using imperfect prediction, demonstrating the effectiveness of the DRCCP.

6.4. Discussion

6.4.1. Key parameter selection

The previous analysis demonstrates the effectiveness of the proposed data-driven method. Such a method contributes to risk avoidance

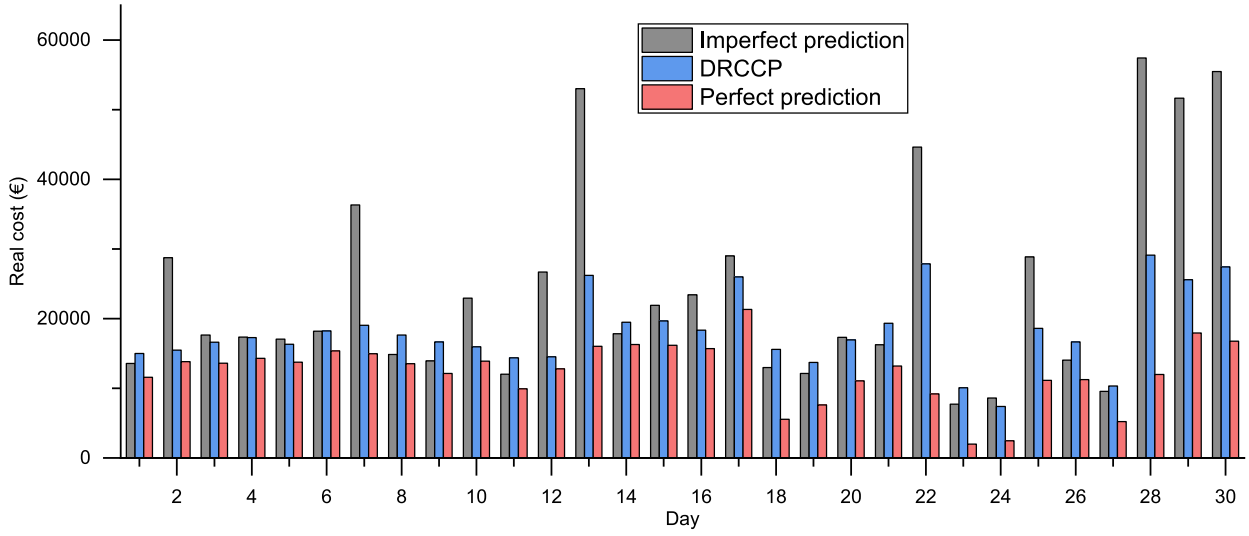

Fig. 6. The resulting real cost from different methods for consecutive 30 operating days.

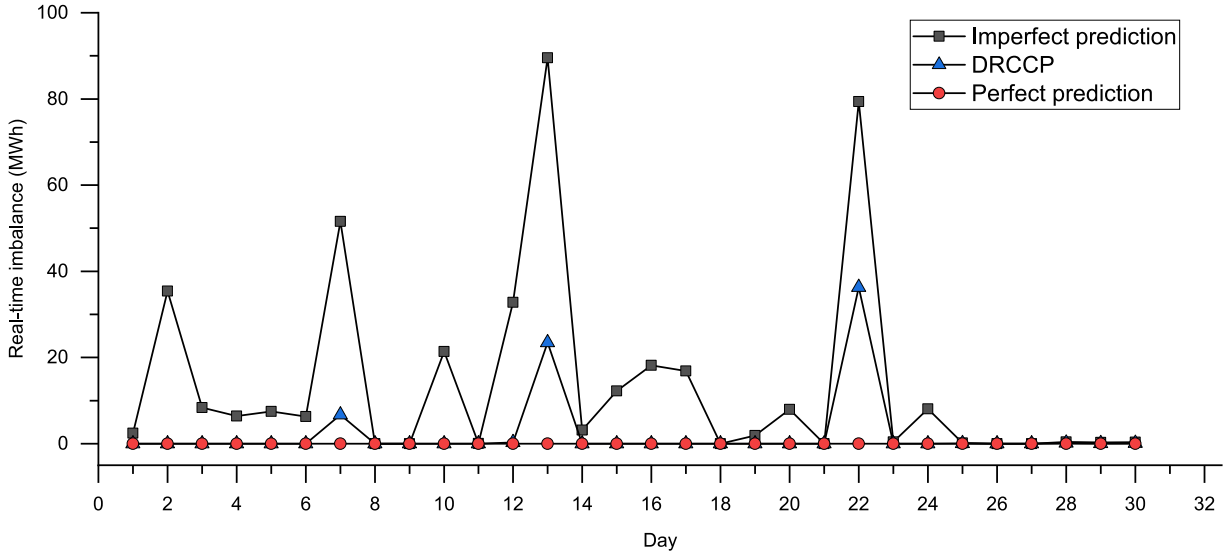

Fig. 7. The resulting real-time energy imbalance from different methods for consecutive 30 operating days.

Table 1
Key operation results in different scenarios.

	Imperfect prediction	Perfect prediction	DRCCP
Operation cost (€)	721 109	370 576	545 427
Real-time imbalance (MWh)	740	0	156

and thus improves the robustness of the decision, and reduces the operation cost. However, it is unclear how the parameter selection for the DRCCP optimization impacts its performance. In a DRCCP optimization, five critical parameters appear, i.e., the probability ϵ_1, radius θ_1 (in constraint (44)), probability ϵ_2, radius θ_2 (in constraint (45)), as well as the number of the samples. The radius shapes the Wasserstein balls where the candidate probability distribution is selected; The probabilities define to which extent the chance constraints should be satisfied; The sample number affects the empirical distribution at the center of the Wasserstein ball.

To reveal the parameters' impacts on the resulting cost of the DRCCP optimization, we again concentrate on day 7 (in Fig. 5(a)). We first change the probability ϵ_1 and radius θ_1, and maintain the remaining parameters. It is found that, from Fig. 8, the optimal cost is not sensitive to the selection of these two parameters. At best, the resulting cost is 18 994€, only 41€ less than the original cost. It implies that the price prediction is not dominant for the cost reduction. One reason is that the price prediction is more accurate than the wind prediction using this specific MLPNN method. Meanwhile, it is the overall price trend and relative changes in a day that dominate the operation strategy. The absolute value plays a less important role. For instance, as observed in Fig. 5(b), although the predicted price generally is smaller than the actual price, they share the similar trends. This feature reduces the requirement of high accuracy prediction.

For wind power prediction, it is found that the related parameters have greater effects on the operation cost. As presented in Fig. 9, the minimum cost is nearly 16 661€ for the best parameter combination ($\epsilon_2 = 0.026$ and $\theta_2 = 0.001$), which is close to the cost from perfect prediction. As the radius of the Wasserstein ball, θ_2 determines the ambiguity set involving the candidate distributions. In general, increasing θ_2 is likely to result in a higher cost for a given relatively small probability. However, the opposite is true for a probability of more than 0.01 in this case. Using a larger radius, we tend to be more conservative and consider the probability distribution distinct

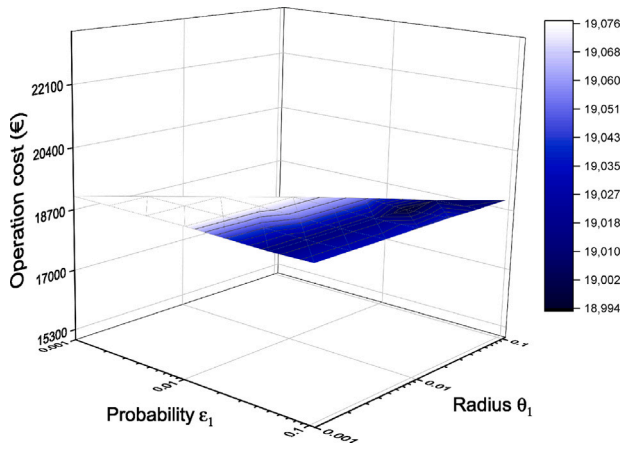

Fig. 8. Resulting actual operation cost using different probability and radius in chance constraint (44).

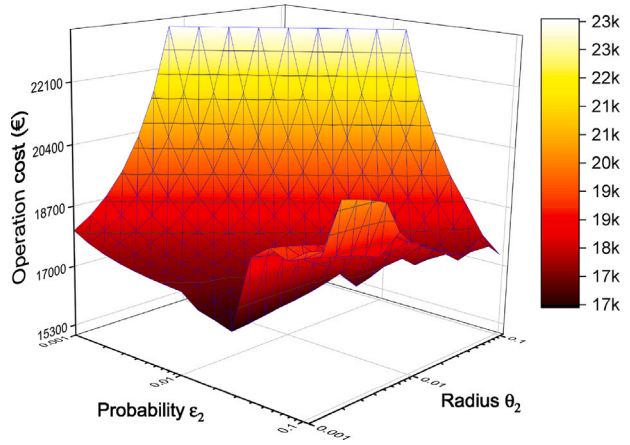

Fig. 9. Resulting actual operation cost using different probability and radius in chance constraint (45).

from the empirical one. The associated risk is that we may include pathological distributions, leading to a poor operation strategy. With a large probability, the influence of pathological distributions is less detrimental since the chance constraints are not strictly satisfied. That is why different phenomena are observed as probability increases.

On the other hand, increasing the probability ϵ_2 can lower the cost given a specific radius, but this is not always true, especially for small radius. ϵ_2 is the probability that the chance constraint can be unsatisfied. Smaller ϵ_2 means that we are more strict with the constraint and more conservative. Fig. 9 suggests that a moderate probability ϵ_2 should be selected to obtain a lower cost. Inappropriate probability can raise the cost by thousands of euros.

It is also found that the optimization becomes infeasible if a small probability and large radius are taken. The infeasibility implies that any decision variable cannot ensure that the chance constraint is satisfied, perhaps due to pathological distributions and strict constraints.

Each historical observation of the prediction errors provides information on the error distribution. It is plausible that more samples are needed for better optimization performance. Fig. 10 illustrates that, in principle, the resulting operation cost diminishes as more samples are used. A sharp decline in operation cost is observed with samples increasing from 1 to 50. However, the curve is neither smooth nor monotonic, and the cost seems to be very sensitive to the chosen samples. The fluctuation becomes smaller when more samples are involved, and the cost remains unchanged if we use more than 100 samples. Contrary to our expectation, the lowest cost is not the stable value but

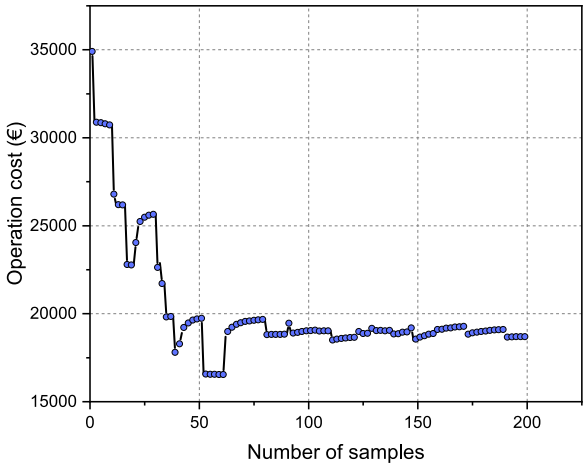

Fig. 10. The minimum cost obtained based on the data-driven method as a function of the sample number.

occurs when the sample number is nearly 50. This is possible because the prediction errors for each day are unlikely to follow identical distribution.

6.4.2. Method comparison

To further discuss the validity of the proposed DRCCP in improving the economic benefits, we compare this method with the traditionally utilized chance constrained programming (CCP). CCP relaxes the constraints in robust optimization and balance the profitability and reliability. It is believed to be a competitive method to solve optimization problems with uncertainties [31]. Problem (43) is rewritten in the following way into CCP:

$$
\begin{aligned}
\min_{\mathbf{x}\in\chi,d}\quad & \mathbf{c}^{\mathrm{T}}\mathbf{x}+d \\
s.t.\quad & \mathbb{P}(\boldsymbol{\xi}^{\mathrm{T}}\mathbf{p}^{u}-d\le 0)\ge 1-\epsilon_1,\quad \forall\boldsymbol{\xi}\in U_{\xi} \\
& \mathbb{P}(p_t^{\mathrm{imb}}\ge p_t^{\mathrm{con}}+p_t^{L}-p_t^{u}-\hat{p}_t^{w}-\zeta_t)\ge 1-\epsilon_2, \\
& \forall\boldsymbol{\zeta}\in U_{\zeta} \\
& \mathbb{P}(p_t^{\mathrm{imb}}\le z_{\mathrm{lps},t}M_2+p_t^{\mathrm{con}}+p_t^{L}-p_t^{u}-\hat{p}_t^{w}-\zeta_t) \\
& \ge 1-\epsilon_2,\quad \forall\boldsymbol{\zeta}\in U_{\zeta}
\end{aligned}
\tag{57}
$$

Different from the chance constraints in DRCCP formulation, the constraints above build on uncertainty sets. For example, the constraint regarding $\boldsymbol{\xi}$ states that the inequality should hold with a probability larger than $1-\epsilon_1$ given any realization of $\boldsymbol{\xi}$ in the uncertainty set U_{ξ}. By scanning the historical forecast errors, we found that the errors, for both wind power and DA electricity price forecast, follow multivariate normal distribution. The components of the random vectors are assumed independent and identically distributed. To be specific, we have $\xi_t \sim \mathcal{N}(0, 10.78^2)$ and $\zeta_t \sim \mathcal{N}(0, 2.68^2)$ in light of statistical properties of the historical data.

It has been widely demonstrated that problem (57) can be solved by mixed integer quadratically-constrained programming given that the uncertainty sets are based on normal distribution. The detailed mathematical derivation is provided in Appendix C.

Fig. 11 illustrates the operation costs for the 30 operating days (the same period in Fig. 6). It is clear that the DRCCP results in fewer operation cost in most days, although the CCP shows better performance in several days. The reason behind this phenomenon is that the CCP tends to be more conservative against uncertainties and loses opportunities for higher revenues. The uncertainty set in CCP only uses a few statistical properties, leading to inefficient usage of historical data. The overall operation cost for the CCP is 560 686€, which is 2.8% higher than the cost in the DRCCP.

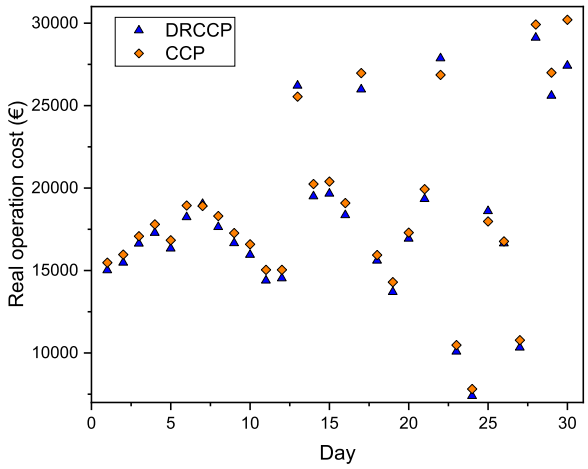

Fig. 11. Operation cost induced by DRCCP and CCP.

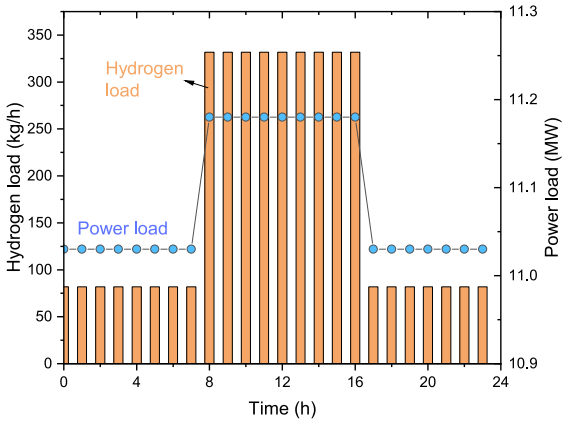

Fig. 12. Hydrogen and power loads during 24-hour operation. This work assumes that the loads remain unchanged for the selected 30 operating days.

7. Conclusion and future work

This work considers a grid-connected wind/hydrogen system with hydrogen storage. The system owner aims at satisfying both the electrical and hydrogen demands at the least operational cost. To make the day-ahead decisions on hydrogen production and power trading, the owner predicts the spot price and wind power output. The decisions are then made based on the constraints from electrolyzer dynamic properties and system operation limits. The prediction, however, is not perfect and brings uncertainty to the system. To handle this problem and enable better decision making, we propose a DDF scheme. The operation problem is formulated as a tractable MILP form.

Although, in general, the prediction is accurate, the results show that the decisions made over the imperfect prediction are poor on some days, which leads to a notable cost rise. The data-driven method significantly reduces the total operation cost for the selected 30 days. An extensive discussion on the parameter selection is then provided. It is found that wind uncertainty is dominant in this specific case. Also, the discussion suggests that a relatively small radius and moderate probability should be adopted for the DRCCP and the sample size needs to be large enough, which should be decided with caution. A comparison between the proposed DRCCP method and traditionally utilized CCP further demonstrates the efficacy of the DRCCP.

Possible future work includes the consideration of the participation in intra-day and real-time markets for such a system. This will make the optimization a multi-stage problem. The prediction will be continually updated, and a rolling optimization or model predicative control method can be adopted. One could also consider electrolysis's providing ancillary service to the grid, which can create extra revenues for a wind/hydrogen system. In another aspect, a probabilistic prediction is relevant to the data-driven method. A good expansion is to replace the deterministic prediction in this paper with a probabilistic prediction for better decision making. Finally, the utilized dynamic electrolysis model can be simplified if there is a need of more efficient computation or the model is used in large-scale problem.

CRediT authorship contribution statement

Yi Zheng: Conceptualization, Methodology, Software, Validation, Writing – original draft, Review & editing. **Jiawei Wang:** Conceptualization, Supervision, Writing – original draft, Review & editing. **Shi You:** Conceptualization, Supervision, Writing – original draft, Review & editing, Funding acquisition. **Ximei Li:** Writing – original draft, Review & editing. **Henrik W. Bindner:** Supervision, Writing – original draft. **Marie Münster:** Supervision, Writing – original draft, Funding acquisition.

Declaration of competing interest

The authors declare the following financial interests/personal relationships which may be considered as potential competing interests: Yi Zheng reports financial support was provided by European Union. Jiawei Wang reports financial support was provided by Villum Foundation.

Data availability

The authors do not have permission to share data.

Acknowledgment

The authors would like to acknowledge financial support from "Synergies Utilizing renewable Power Regionally by means of Power To Gas project", which received funding in the framework of the joint programming initiative ERA-Net Smart Energy Systems' focus initiative Integrated, Regional Energy Systems, with support from the European Union's Horizon 2020 research and innovation program under grant agreement No 775970. This work is also funded by a research grant (37177) from VILLUM FONDEN, Denmark. Project title: Data-driven Approaches for enhancing resilience of Multi-Energy systems (DAME).

Appendix A. Power and hydrogen loads

The power and hydrogen loads are shown in Fig. 12.

Appendix B. System critical parameters

The system critical parameters can be found in Table 2.

Appendix C. Reformulation of chance constrained programming

For better readability, we repeat problem (57) here:

$$\min_{\mathbf{x}\in\chi,d} \quad \mathbf{c}^{\mathrm{T}}\mathbf{x}+d \tag{58}$$

$$s.t. \quad \mathbb{P}(\boldsymbol{\xi}^{\mathrm{T}}\mathbf{p}^{u}-d\le 0)\ge 1-\epsilon_1, \quad \forall\boldsymbol{\xi}\in U_{\xi} \tag{59}$$

$$\mathbb{P}(p_t^{\mathrm{imb}}\ge p_t^{\mathrm{con}}+p_t^{L}-p_t^{u}-\hat{p}_t^{w}-\zeta_t)\ge 1-\epsilon_2, \quad \forall\boldsymbol{\zeta}\in U_{\zeta} \tag{60}$$

$$\mathbb{P}(p_t^{\mathrm{imb}}\le z_{\mathrm{lps},t}U+p_t^{\mathrm{con}}+p_t^{L}-p_t^{u}-\hat{p}_t^{w}-\zeta_t)\ge 1-\epsilon_2, \quad \forall\boldsymbol{\zeta}\in U_{\zeta} \tag{61}$$

Table 2
The critical system parameters.

Parameter	Value	Parameter	Value	Parameter	
Wind turbine					
Hub height	150 m	Cut-in speed	3 m/s	Rate speed	14.32 m/s
Cut-out speed	22.5 m/s	Rotor diameter	150 m	Rated power	4.2 MW
Hellman coefficient	0.128				
Electrolyzer					
Power consumption at 100% load	48.1 kWh/kg	Power consumption at 50% load	45 kWh/kg	Power consumption at 25% load	42.7 kWh/kg
Total area of the stack	43.14 m^2	Minimal current density	1000 A/m^2	Maximal current density	5000 A/m^2
Number of the stacks	12				
Others					
Hydrogen tank size	6000 kg	SoC lower limit	0.1	SoC upper limit	0.9
Initial SoC	0.5	Converter efficiency	0.95	Compressor coefficient β	3.7×10^{-4} MWh/kg

We already have $\xi_t \sim \mathcal{N}(0, 10.78^2)$ and $\zeta_t \sim \mathcal{N}(0, 2.68^2)$. It can be inferred that $\boldsymbol{\xi} \sim \mathcal{N}(\mathbf{0}, \Sigma)$, where Σ is the covariance matrix, a diagonal matrix since the components are independent and identically distributed. Let $\psi = \boldsymbol{\xi}^{\mathrm{T}}\mathbf{p}^u - d$, then for fixed $\mathbf{p}^u$ and d:

$$\psi \sim \mathcal{N}(-d, \mathbf{p}_u^T \Sigma \mathbf{p}_u) \tag{62}$$

Let U be a random variable following $\mathcal{N}(0, 1)$, we then get:

$$\psi = -d + \sqrt{\mathbf{p}_u^T \Sigma \mathbf{p}_u} U = -d + \sigma U \tag{63}$$

Constraint (58) is equivalent to:

$$\mathbb{P}(-d + \sigma U \le 0) \ge 1 - \epsilon_1 \tag{64}$$

$$\mathbb{P}(U \le \frac{d}{\sigma}) \ge 1 - \epsilon_1 \tag{65}$$

Denote $\Phi(u)$ as the cumulative distribution function of U:

$$\Phi(u) = \mathbb{P}(U \le u) = \frac{1}{\sqrt{2\pi}} \int_{-\infty}^{u} e^{-\frac{t^2}{2}} dt \tag{66}$$

Then, we can rewrite inequality (65) as:

$$d \ge \Phi^{-1}(1 - \epsilon_1)\sigma \tag{67}$$

For a pre-specified ϵ_1, $\Phi^{-1}(1-\epsilon_1)$ is simply a constant. Since $\sigma = 10.78 \parallel \mathbf{p}_u \parallel_2$ in this specific problem, the constraint above has a second-order cone form.

Similar derivation gives tractable form of constraints (60) and (61) as:

$$p_t^{\mathrm{con}} + p_t^L - p_t^u - \hat{p}_t^w - p_t^{\mathrm{imb}} \le 2.68\Phi^{-1}(\epsilon_2) \tag{68}$$

$$z_{\mathrm{lps},t} M_2 + p_t^{\mathrm{con}} + p_t^L - p_t^u - \hat{p}_t^w - p_t^{\mathrm{imb}} \ge 2.68\Phi^{-1}(1 - \epsilon_2) \tag{69}$$

The above reformulation enables the problem to be a tractable mixed integer quadratically constrained programming and to be also solved by commercial solvers, such as Gurobi.

References

[1] Gielen D, Taibi E, Miranda R. Hydrogen: A renewable energy perspective. Abu Dhabi: International Renewable Energy Agency; 2019.

[2] Weimann L, Gabrielli P, Boldrini A, Kramer GJ, Gazzani M. Optimal hydrogen production in a wind-dominated zero-emission energy system. Adv Appl Energy 2021;3:100032.

[3] Shaner MR, Atwater HA, Lewis NS, McFarland EW. A comparative technoeconomic analysis of renewable hydrogen production using solar energy. Energy Environ Sci 2016;9(7):2354–71.

[4] Nguyen T, Abdin Z, Holm T, Mérida W. Grid-connected hydrogen production via large-scale water electrolysis. Energy Convers Manage 2019;200:112108.

[5] Guerra OJ, Eichman J, Kurtz J, Hodge B-M. Cost competitiveness of electrolytic hydrogen. Joule 2019;3(10):2425–43.

[6] James B, DeSantis D, Saur G. Final report: hydrogen production pathways cost analysis (2013–2016). US department of energy report DOE-StrategicAnalysis-6231-1, 2016.

[7] IEA. The future of hydrogen. 2019, https://www.iea.org/reports/the-future-of-hydrogen.

[8] NordPool. Day-ahead market. 2022, https://www.nordpoolgroup.com/the-power-market/Day-ahead-market/, Accessed: 2022-03-01.

[9] He G, Chen Q, Kang C, Xia Q, Poolla K. Cooperation of wind power and battery storage to provide frequency regulation in power markets. IEEE Trans Power Syst 2016;32(5):3559–68.

[10] Almansoori A, Shah N. Design and operation of a stochastic hydrogen supply chain network under demand uncertainty. Int J Hydrogen Energy 2012;37(5):3965–77.

[11] Mei J, Zuo Y, Lee CH, Wang X, Kirtley JL. Stochastic optimization of multi-energy system operation considering hydrogen-based vehicle applications. Adv Appl Energy 2021;2:100031.

[12] Xu X, Hu W, Liu W, Zhang Z, Du Y, Chen Z, Abulanwar S. Optimal operational strategy for a future electricity and hydrogen supply system in a residential area. Int J Hydrogen Energy 2022;47(7):4426–40.

[13] Li B, Roche R, Paire D, Miraoui A. Sizing of a stand-alone microgrid considering electric power, cooling/heating, hydrogen loads and hydrogen storage degradation. Appl Energy 2017;205:1244–59.

[14] Coppitters D, Verleysen K, De Paepe W, Contino F. How can renewable hydrogen compete with diesel in public transport? Robust design optimization of a hydrogen refueling station under techno-economic and environmental uncertainty. Appl Energy 2022;312:118694.

[15] Yang J, Su C. Robust optimization of microgrid based on renewable distributed power generation and load demand uncertainty. Energy 2021;223:120043.

[16] Zheng QP, Wang J, Liu AL. Stochastic optimization for unit commitment—A review. IEEE Trans Power Syst 2014;30(4):1913–24.

[17] Zhao C, Guan Y. Data-driven stochastic unit commitment for integrating wind generation. IEEE Trans Power Syst 2015;31(4):2587–96.

[18] Zhu R, Wei H, Bai X. Wasserstein metric based distributionally robust approximate framework for unit commitment. IEEE Trans Power Syst 2019;34(4):2991–3001.

[19] Ji R, Lejeune MA. Data-driven distributionally robust chance-constrained optimization with Wasserstein metric. J Global Optim 2021;79(4):779–811.

[20] Khalil Alsmadi M, Omar KB, Noah SA, Almarashdah I. Performance comparison of multi-layer perceptron (Back Propagation, Delta Rule and Perceptron) algorithms in neural networks. In: 2009 IEEE international advance computing conference. IEEE; 2009, p. 296–9.

[21] Abiodun OI, Jantan A, Omolara AE, Dada KV, Mohamed NA, Arshad H. State-of-the-art in artificial neural network applications: A survey. Heliyon 2018;4(11):e00938.

[22] Zheng Y, You S, Bindner HW, Münster M. Incorporating optimal operation strategies into investment planning for wind/electrolyser system. CSEE J Power Energy Syst 2022;1–13. http://dx.doi.org/10.17775/CSEEJPES.2021.04240.

[23] Zheng Y, You S, Bindner HW, Münster M. Optimal day-ahead dispatch of an alkaline electrolyser system concerning thermal–electric properties and state-transitional dynamics. Appl Energy 2022;307:118091.

[24] Wei W, Wang J. Modeling and optimization of interdependent energy infrastructures. Springer; 2020.

[25] Matute G, Yusta JM, Beyza J, Correas LC. Multi-state techno-economic model for optimal dispatch of grid connected hydrogen electrolysis systems operating under dynamic conditions. Int J Hydrogen Energy 2021;46(2):1449–60.

[26] Buttler A, Spliethoff H. Current status of water electrolysis for energy storage, grid balancing and sector coupling via power-to-gas and power-to-liquids: A review. Renew Sustain Energy Rev 2018;82:2440–54.

[27] Bertuccioli L, Chan A, Hart D, Lehner F, Madden B, Standen E. Study on development of water electrolysis in the EU. Fuel Cells Hydrog Joint Undert 2014;1–160.

[28] Ben-Tal A, El Ghaoui L, Nemirovski A. Robust optimization. Princeton University Press; 2009.

[29] Xie W, Ahmed S. On deterministic reformulations of distributionally robust joint chance constrained optimization problems. SIAM J Optim 2018;28(2):1151–82.

[30] Chen Z, Kuhn D, Wiesemann W. Data-driven chance constrained programs over Wasserstein balls. 2018, arXiv preprint arXiv:1809.00210.

[31] Zhang H, Li P. Chance constrained programming for optimal power flow under uncertainty. IEEE Trans Power Syst 2011;26(4):2417–24.